Design and Pilot Evaluation of an Ungrounded Force Perturbation Device

by

Niels Doup

to obtain the degree of Master of Science
at the Delft University of Technology,
to be defended publicly on the 25th of March 2025

Student number: 4866193

Thesis committee:	Dr. ir. A. H. A. Stienen,	TU Delft, supervisor
	ir. J. C. van Zanten,	TU Delft, supervisor
	Dr. ir. M. L. van de Ruit,	TU Delft, graduation committee member
	ir. C. S. ter Welle,	TU Delft, graduation committee member

TU Delft

CONTENTS

Design and Pilot Evaluation of an Ungrounded Force Perturbation Device for Elbow Joint Dynamics Assessment

Niels Doup

***Abstract*— Stroke survivors often exhibit motor impairments, which hinder activities of daily living. While grounded robotic perturbation devices can accurately quantify joint dynamics via system identification, their size and fixed positioning limit functional assessments under realistic conditions. To address this gap, we present the design and pilot evaluation of a novel, wearable perturbation device capable of delivering ungrounded force perturbations to the user's forearm.**

The device uses a linear solenoid actuator housed in a wrist brace to generate short, pulse-type forces, thereby inducing small angular deflections (approximately 1–3°) to the arm. An inertial measurement unit (IMU) placed on the brace tracks the resulting movement, while an accelerometer on the solenoid coil measures the perturbation force. Nine healthy participants performed three tasks—relax, resist, and move. Random pulse signals were used to prevent anticipation of the perturbations. The device successfully deflected the arm in all tasks. The largest deflections was recorded during the relax task and smaller, though still measurable, deflections in the resist and move tasks.

Estimated stiffness values in each task indicated that the device could distinguish different levels of joint rigidity, although comparisons with established literature showed some over- or underestimation. Factors such as non-rigid brace attachment and off-center actuator placement contributed to these discrepancies. Despite these limitations, the prototype demonstrates the feasibility of wearable, ungrounded force perturbations for assessing elbow dynamics. Future work will focus on improving the device's rigidity, exploring multi-degree-of-freedom perturbations, and refining stiffness estimation algorithms to better capture realistic joint behaviors.

***Index Terms*— Elbow joint dynamics, mechatronic design, ungrounded perturbation**

I. Introduction and Background

Stroke is the second leading cause of death and the third leading cause of disease burden worldwide [1]. A stroke occurs when the brain experiences reduced blood flow, leading to cell death. This damage often results in injuries to the central nervous system (CNS), particularly the upper motor neurons (UMN), which are responsible for initiating and modulating voluntary movement [2]. Damage to these neurons can cause a range of symptoms, including muscle weakness, spasticity, hyperreflexia, abnormal synergies, and changes in viscoelastic muscle properties. When these motor impairments affect the upper limb, they can significantly interfere with daily activities such as reaching and grasping [3].

Clinically, spasticity of joints of stroke patients is often estimated using the Modified Ashworth Scale (MAS) or the Modified Tardieu Scale (MTS) [4, 5]. In these methods, a physician stretches the patient's limb and scores the perceived resistance on a scale from 0 to 4 or 5. However, these methods have notable limitations. They do not give information about joint impedance and their limited scales fail to provide detailed information about specific properties such as damping and stiffness. Additionally, concerns have been raised about the intra-rater reliability of these tests [6, 7].

Accurate prognosis and tailored neurorehabilitation are essential for the recovery of stroke patients. To achieve this, it is crucial to precisely quantify and classify motor impairments [8, 9]. The dynamic properties of a joint are often refereed to with the term 'joint impedance'. Impedance refers to the resistance of a joint in response to a rotational movement or torque, and is typically modeled as a combination of inertia, rotational stiffness, and damping [10].

A. Robotic devices

Several robotic devices have been developed over the recent years, that could address the limitations of these clinical scales. These devices have proven been effective in accurately quantifying the impedance of a joint, some by utilizing a methodology called system identification. System identification is a technique that builds a model of a system by measuring its output in response to a known input [10]. For robotic devices, this typically involves stretching a joint and measuring the resistance it generates in response, these stretches are often referred to as perturbations.

Various types of perturbation signals are used in system identification [11]. The simplest method is the ramp-and-hold signal [12, 13], in which the device stretches the joint to a specific angle and holds it there, mimicking the assessments performed by clinicians. Another commonly used perturbation signal is the sinusoidal type. This includes white noise signals or multisine signals that combine multiple sinusoidal frequencies [14, 15]. Lastly, pulse-type signals are also used. These binary signals toggle between on and off states in a predefined pattern or as a pseudo-random binary sequence (PRBS) [16, 17].

One example of a robotic perturbation device is the Shoulder-Elbow-Perturbator (SEP) [18], shown in Figure 1 (left). This device stretches the elbow joint while passively supporting part of its weight and can deliver both ramp-and-hold and multisine perturbations. Another example is the Proprio, shown in Fig. 1 (right) [19]. This one-degree-of-freedom (1-DOF) perturbator provides force perturbations through a handle held by the user, with the elbow positioned at 90 degrees of flexion. This setup enables measurements of shoulder joint properties.

Fig. 1: On the left: the shoulder-elbow-perturbator (SEP) on the right: the Proprio [15, 18]

Despite their accuracy, existing perturbation devices have notable limitations. Their grounded nature restricts measurements to specific positions. For instance, the SEP requires participants to sit next to the device with their shoulder abducted at 90 degrees, making it unsuitable for assessing joint properties during functional tasks like reaching or grasping. These activities are particularly important to study, as joint properties can vary with posture and muscle activation levels [20, 21]. To overcome these limitations, a new type of ungrounded perturbation device is needed—one capable of delivering force perturbations to the user's upper limb in various contexts without relying on external frame or base.

B. Research Goal

The goal of this paper will be to present a new design of an ungrounded perturbation device, capable of delivering force perturbations to the forearm.

For effective joint dynamics estimations, the limb's positional displacement in response to a perturbation must be large enough to be reliably measured, yet small enough to maintain a valid linear approximation of the system. Previous studies have indicated that a deflection of around 0.03 rad (approximately 1.7°) typically meets these criteria [22, 23]. Therefore, the following research question has been formulated: *Can the presented design deflect the underarm, in the flexion/extension direction, for 1.7 degrees during various tasks?*

To find an answer to this question, an actuation mechanism that generates ungrounded perturbation will be selected and a prototype containing this mechanism will be made. To tests its perturbation capabilities during various tasks, an experiment involving human subjects will be set up and conducted. The arm orientation results will be analyzed and stiffness values of the arm will be estimated.

II. Material and Methods

A. Ungrounded force generation mechanisms

For a perturbation device to be ungrounded, an actuation mechanism that can generate ungrounded forces must be included. Over recent years, various ungrounded force feedback systems have been developed, particularly in the context of perturbation devices as well as virtual reality applications [24]. These mechanisms can be broadly categorized into three main types: mechanisms that rotate a mass, mechanisms that move a mass linearly, and mechanisms that use air propulsion. A more detailed overview of these mechanisms can be seen in Appendix I as well as the functional criteria that a concept needs to include for it to be successful concept. The most important functional criteria for an ungrounded device are:

- It must be able to give ungrounded force perturbations to the forearm.
- It must allow for the range of motion of the elbow of 140° from fully flexed position to fully extended position.
- It must not weigh more than 500 grams.
- It must be able to measure the input force as well as the output dynamics.

Not all mechanisms are suitable to be used for an arm-worn perturbation device. Some are too bulky or too heavy, for example. The most promising mechanisms were compared using the weighted criteria method. Criteria for this selection were mass, number of parts, intrusiveness and number of parts readily available. The three mechanisms that scored the highest were the ones that used Bowden cables, a torque motor, and a linear electric actuator such as a voice coil actuator or solenoid.

As said before, the aim for this perturbation device will be to cause an arm rotation of around 1.7 degrees. Perturbations that are much larger than this are undesirable, since impedance is position depended so larger stretches could cause nonlinearities in the estimated system [25]. To estimate the power requirements for achieving such a deflection, the power of a single perturbation was modeled for each actuation mechanism (Appendix I-A). Although the calculations indicated that the linear actuator concept required more power to achieve the same deflection compared to the other two concepts, all mechanisms were within the reasonable power range of commercially available actuators.

Bowden cables are known to introduce significant friction into the system. Consistent with findings in [26], friction losses in Bowden cables can account for up to 33% of energy loss during power transmission from the actuator to the joint. Moreover, this friction is influenced by the curvature of the cables, making it inconsistent during activities of daily living (ADL), where cable bending is likely. Using a torque motor, on the other hand, would require a rigid connection between the forearm and upper arm. This setup would not only require a complex control scheme but also restrict wrist pronation and supination. Given these considerations,

the chosen actuation principle for the prototype is a linear electric actuator.

B. Prototype

The principle behind this concept states that when a mass accelerates or decelerates, it produces a force that opposes the change in motion which acts upon the entire system. To test the feasibility of using a linear electric actuator as a perturbation device, a prototype was developed, as shown in Figure 3.

The prototype features a linear solenoid (WANGCL FJ-Z05 DC 12V 2.5A) designed to generate a force of up to 45 N at its rated current and voltage of 2.5 A and 12 V, respectively (see Appendix II for actuator comparison). The solenoid is housed within a casing that fixates both ends of the plunger. This configuration ensures that, when powered, the coil of the solenoid moves instead of the plunger.

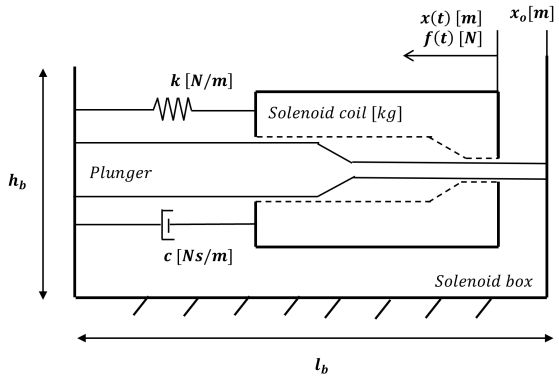

Fig. 2: Schematic overview of the key parameters of the solenoid system.

Fig. 2 illustrates the system's parameters and kinematics. The motion of the solenoid can be described by a second order differential equation 1. With m $[kg]$, b $[Ns/m]$, and k $[N/m]$ the mass of the coil of the solenoid, the damping caused by the friction of the bearings and the stiffness of the return spring. $f(t)$ $[N]$ represents the electromagnetic force that is applied and $x(t)[m]$ is the position of the solenoid coil. The inertial component $m\ddot{x}(t)$ will cause the reaction force transferred to the arm.

$$f(t) = m\ddot{x}(t) + b\dot{x}(t) + kx(t) \tag{1}$$

Furthermore, a commercially available hand-wrist brace (Offtrte B0C6Z7R8DV) was used for this prototype, as the mounting platform for the solenoid. This brace, often prescribed for carpal tunnel syndrome, features a sleeve and three parallel aluminum splints (one on the bottom of the wrist and two on the sides) to keep the wrist aligned. The solenoid assembly was attached to the bottom splint of the brace.

To measure the underarm's acceleration response to the applied perturbation, an inertial measurement unit (IMU)

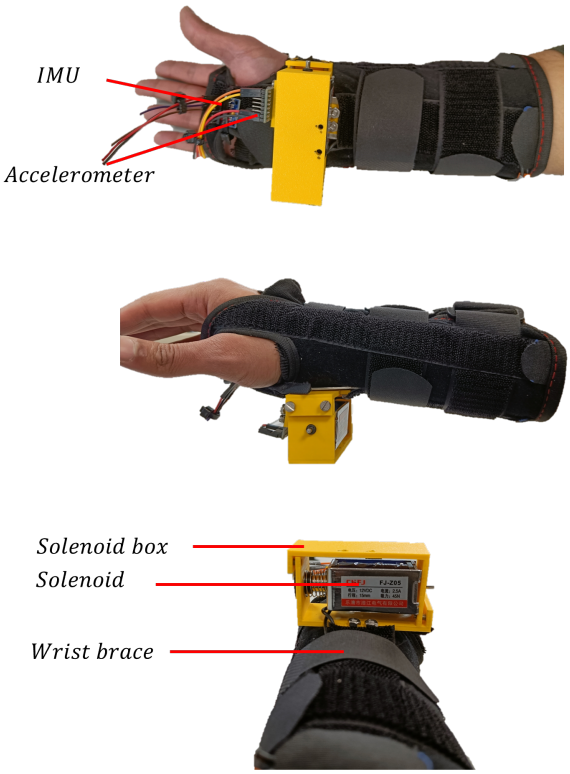

Fig. 3: Bottom, side and front views of the prototype including the primary components

Dimensions solenoid (l_s x w_s x h_s) (mm)	50 x 30 x 25
Dimensions solenoid box (l_b x w_b x h_b) (mm)	70 x 30 x 44
Stroke length (mm)	15
Solenoid mass (g)	191
Solenoid Coil (the moving mass) (g)	156
Total mass (g)	325

TABLE I: Relevant parameters of the concept

(MPU6050) was attached at the distal end of the brace. This sensor measures both linear acceleration and angular velocity. An accelerometer (ADXL345 $\pm$16g) was mounted on the solenoid's moving coil to measure its acceleration directly as well as the timing and duration of the perturbation. Because the coil mass is known, multiplying the measured coil acceleration by the mass yields the applied perturbing force.

The solenoid controller was implemented using MATLAB 2022b, with processing handled by a micro controller (Seeeduino Nano). Sensor data collected by the controller was saved locally and anonymously in .mat files. To achieve higher forces, an external adjustable power supply delivered power to the solenoid with a voltage of 32 V and a current of 3 A (the full electric wiring, including the components, can be seen in appendix III). Since the solenoid was only activated in short pulses, operating it at a higher voltage and

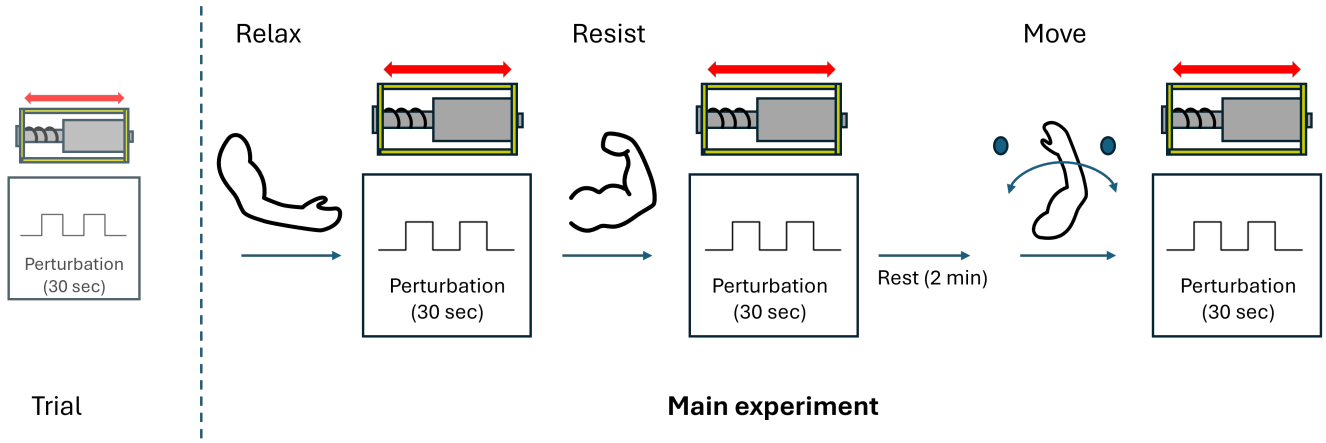

Fig. 4: Flow diagram with the tasks that the participants are asked to perform during the experiment. The main experiment consists of three task: relax, resist and move. Each task lasted 30 seconds and was performed twice.

current was deemed safe. Key parameters of the system are summarized in Table I.

C. Experimental Setup

1) Research Goal: The goal of the experimental procedure was to determine whether the wearable perturbation device could produce sufficiently large perturbations (around 0.03 rad, or 1.7°) under different task conditions. In addition, to assess whether the device could estimate joint impedance parameters during these tasks, stiffness values were calculated. Because this was a pilot study, the focus was limited to stiffness, excluding other impedance parameters.

2) Experimental Procedure: Before the experiment begins, the brace is securely fitted onto the dominant arm of the participant. Since the primary focus of this study is the elbow joint and the lower-arm inertia, the weight of the arm was compensated and the shoulder motion restricted. To achieve this, the participant's arm is placed in a gravity-compensating arm holder (SaeboMAS mini). The arm was placed so that the back of the arm support was aligned with the medial head of the epicondyle. The arm holder itself was adjusted to ensure the participant's arm remains elevated and does not make contact with the desk. It also made sure that the arm of each participant was in the same position and alligned with the horizontal plane. To ensure the participants safety, an emergency button was integrated into the system. Pressing it by the participant or researcher would immediately cut the power to the solenoid.

To familiarize the participant with the setup and perturbation strength, a trial run is conducted before the main experiment. The main experimental protocol, which can be seen in Fig. 4, consists of three parts:

1) *Relax task:* In the first part the participant is instructed to fully relax their arm, allowing the perturbations to move it without resistance.
2) *Resistive Task:* In the second part, the participant is instructed to fully flex their arm and resist the applied perturbations as much as possible.

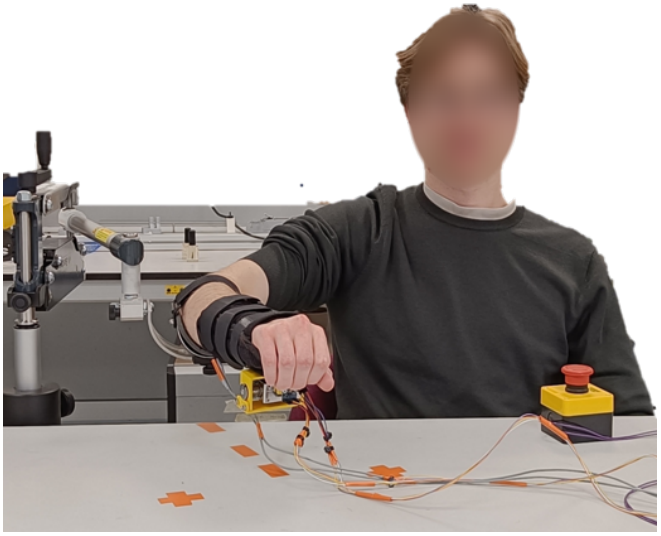

Fig. 5: A typical overview of a participant seated in the experimental setup. Line markings on the desk show where they keep their arm during the relax and resist task. Cross markings show the endpoints of the move task.

3) *Dynamic Task:* In the final part, the participant moves their arm from left to right and back again between two markings placed on the desk in front of them, synchronized with a metronome that gives an auditory signal every 2 seconds. The markings were place within 20 degrees from the centerline. This dynamic task simulates a scenario closer to activities of daily living (ADLs) and evaluates whether the applied perturbations can deviate the arm during movement.

The full step-by-step protocol of all the actions that were performed before, during and after the experiment can be seen in Appendix IV.

For all three tasks, a random pulse signal is applied to the wearable perturbator to prevent the participant from anticipating the perturbations, ensuring that natural responses

are captured. This random binary signal alternates between 0 and 1, controlling a resistor that engages or disengages the solenoid. Each pulse lasted 0.15 s to ensure full solenoid contraction. An example of such a random signal is seen in Fig. 6. To further prevent anticipation of the perturbations the random signal varied between the three tasks. The signals were kept the same across participants for better comparison and analysis. All three tasks were performed twice for each participant to minimize the risk of data loss and to gather sufficient enough data.

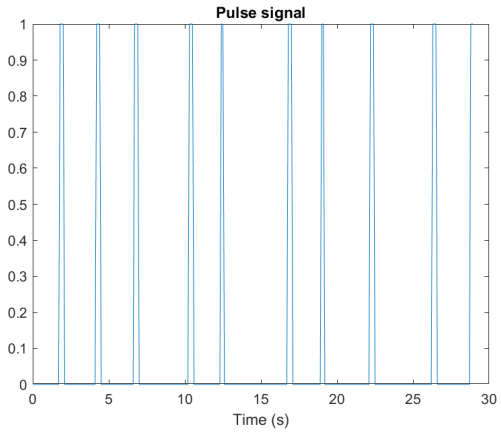

Fig. 6: An example of the random pulse signal that was given as an input to the micro controller that controls the solenoid

To mitigate muscle fatigue, which can reduce muscle force during the resistive task, the duration is limited to 30 seconds for each task. This duration has been shown to be suitable for similar experiments [27]. Additionally, a rest period of 2 minutes is provided between the resist tasks to further minimize fatigue.

D. Participants

The experiment involved n = 9 participants, comprising 5 males and 4 females and they were all right-handed. All participants were healthy adults aged 22–27 years with a mean age of 24.1 years old, with no known arm impairments.

Before participating, each individual received detailed information about the experiment, including the data that would be collected and any potential risks involved. Informed consent was obtained from each participant prior to the start of the experiment (Appendix VI-VII).

E. Data processing

The acceleration and gyroscopic data that was measured by the IMU and the acceleration data of the accelerometer were all stored separately in Nx3 matrices. N being the number of samples collected, in m/s^2 or deg/s, and each row representing a principle axis (XYZ). The sampling rate of the sensors was set to 200 Hz (interval of 0.005 s), which is the maximum rate the I2C connection of the micro controller with Matlab would allow. However due to execution speed of the loop and possible communication latency the sampling rate in reality was slightly lower. The full script that was

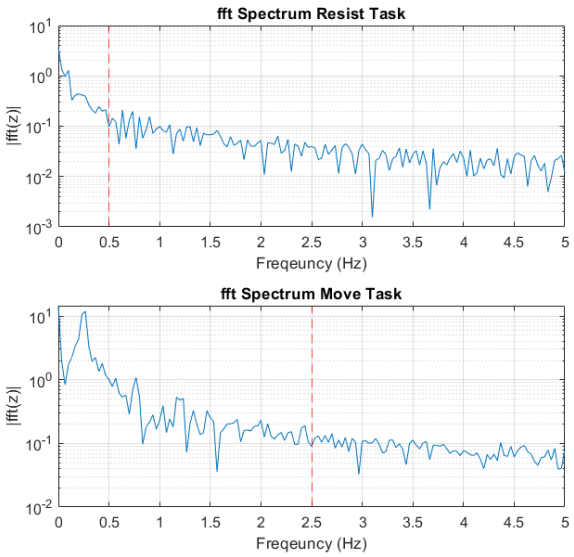

Fig. 7: Fast Fourier Transform (fft) spectra of the orientation data of the resist and move task. The red dashed line represents the cut-off frequency that was chosen to compensate the drift. The fft of the relax task is not shown however it showed similar results as the resist task.

used to collect all the data of the participants can be seen in Appendix VIII . All arrays were resampled to 200 Hz using a polyphase anti-aliasing filter.

To get an estimate of the orientation of the arm, a Kalman filter (*imufilter* function in MATLAB) was used which fused the acceleration and gyroscopic data collected by the IMU. In Fig. 8 a typical orientation estimate of the sensor data can be seen. The figure shows that there was drift present in the orientation estimate. To verify that low frequency components contributed to this drift the Fast Fourier Transform (fft) was investigated which can be seen in Fig. 7. It can be seen that there is a high magnitude present for frequencies below 0.5 Hz for the relax and resist task. To remove this drift, and also high frequency noise, the data was filtered using a band-pass fourth-order Butterworth filter with a low cut off frequency of 0.5 Hz and a high cutoff frequency of 40 Hz. For the move task it can be seen that there was more drift present up to frequencies of 2.5 Hz, so for these datasets a low cutoff of 2.5 Hz was chosen.

To determine how much the arm moves in response to a perturbation, the minimum and the maximum $(\theta_{min}, \theta_{max})$ orientation at each perturbation instance was recorded and the difference between these orientations was computed.

F. Additional experiments

To investigate the magnitude and duration of the perturbing force, the accelerometer data from the solenoid coil were analyzed for ten perturbations applied during the resist task. The force generated was calculated as the product of the coil's mass and its measured acceleration.

Next, the maximum achievable perturbation frequency in

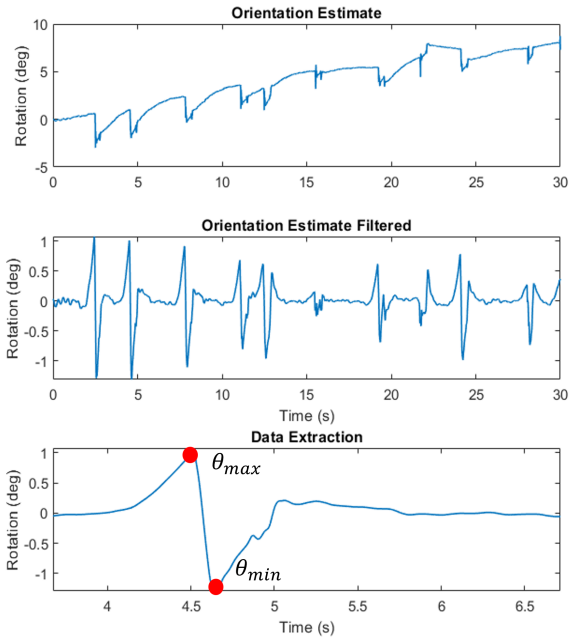

Fig. 8: Top: typical graph of the orientation of the arm during the relax task with drift present. Middle: Drift filtered out with a high pass filter. Bottom: Data which was extracted from each perturbation. Data was smoothed for clarity.

different solenoid orientations was evaluated by gradually increasing the contraction frequency by 0.5 Hz increments, starting from 1 Hz. The test ended when the solenoid coil could no longer strike the end of its enclosure. This procedure was repeated in three orientations: horizontal, vertical (spring above the coil), and upside-down vertical (spring below the coil).

G. Stiffness estimation

The orientation and acceleration data that was gathered has been used to get estimates of the stiffness values per task. This was done following a similar approach as Yagi et al. in [28, 29]. First, the elbow joint is assumed to be described by a linear model:

$$\tau(t) = I\ddot{\theta}(t) + B\dot{\theta}(t) + K\theta(t) \tag{2}$$

Where $\tau(t)$ is the applied torque perturbation [Nm], I, b and k are the joint inertia [kg*m^2], rotational damping [Nms/rad] and rotational stiffness [Nm/rad], respectively. Furthermore, $\ddot{\theta}, \dot{\theta}$ and θ are the joint angular acceleration, velocity and position. Because a digital signal processor is used, a parametric linear difference equation is needed described as:

$$\theta_k = a_1\theta_{k-1} + a_2\theta_{k-2} + b_0\tau_k + b_1\tau_{k-1} + b_2\tau_{k-2} \tag{3}$$

Where a_1, a_2, b_0, b_1 and b_2 are the parameters that need to be estimated, and k is the time step. According to Yagi et al. in [30] we can relate equation 2 and 3 to each other to derive the stiffness value:

$$K = \frac{1 - a_1 - a_2}{b_0 + b_1 + b_2} \tag{4}$$

To find a_1, a_2, b_0, b_1 and b_2, the following equation can be solved:

$$\phi = (G^T G)^{-1} G^T \Theta \tag{5}$$

Where

$$\phi = [a_1 \quad a_2 \quad b_0 \quad b_1 \quad b_2]^{\mathrm{T}},$$
$$\Theta = [\theta_1 \quad \theta_2 \quad \theta_3 \quad \cdots \quad \theta_N]^{\mathrm{T}},$$
$$G = \begin{bmatrix} 0 & 0 & \alpha & 0 & 0 \\ \theta_1 & 0 & 0 & \alpha & 0 \\ \theta_2 & \theta_1 & 0 & 0 & \alpha \\ \theta_3 & \theta_2 & 0 & 0 & 0 \\ \vdots & \vdots & \vdots & \vdots & \vdots \\ \theta_{N-1} & \theta_{N-2} & 0 & 0 & 0 \end{bmatrix},$$

Where α is constant based on the area of the input torque $\tau(t)$. A more detailed explanation as well as the calculation of constant α can be seen in Appendix IX.

Since the actuator is placed below the wrist, this will also generate a torque around the pronation/supination axis of the underarm and therefore also a rotation in that direction instead of the flexion/extension direction of the elbow. To account for the motion in this direction, it will be subtracted from the the measured angle and the resulting angle can than be described as followed:

$$\theta_N = \sin^{-1}\frac{r\sin(\psi_N) - w\sin(\gamma_N)}{r} \tag{6}$$

Where ψ_N is the measured angle in the flexion/extension direction of the elbow, γ_N is the measured angle in the pronation/supination direction, r and w the wrist to elbow length and the radius of wrist respectively. For these lengths, the average lengths of 29 cm and 2.2 cm will be used [31, 32]. The stiffness will be estimated for each perturbation individually, sorted by task.

III. Results

A. Results of the Experiments

An overview of the orientation data per task for all participants and trials is shown in Fig. 9. The blue line represents the mean of all the trials, and the shaded blue area represents the standard deviation. For the first two graphs (relax and resist tasks), sensor drift has been filtered out using a band-pass filter as described earlier. It can be seen that the perturbations in the relax and resist tasks are clearly visible in the average orientation results.

The perturbations in the move task are not clearly visible initially, but after filtering out the movement, they become apparent. Because the data for the move task was significantly noisier than that for the other two tasks and more drift was present, a higher cut-off frequency was chosen to

visualize the perturbations, as shown in Fig. 10. During the move task, some human errors occurred. In the recordings of the move task, four trials were excluded for this reason, as they were either out of sync or did not show a sinusoidal signal, as described in Appendix X.

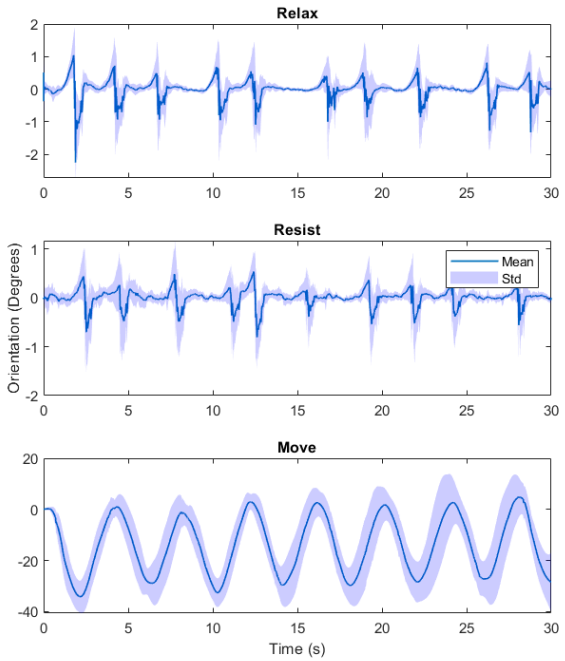

Fig. 9: Overview of all the orientation data around the z-axis of all participants and trials per task. The blue line represents the mean of the data and the shaded blue area its standard deviation.

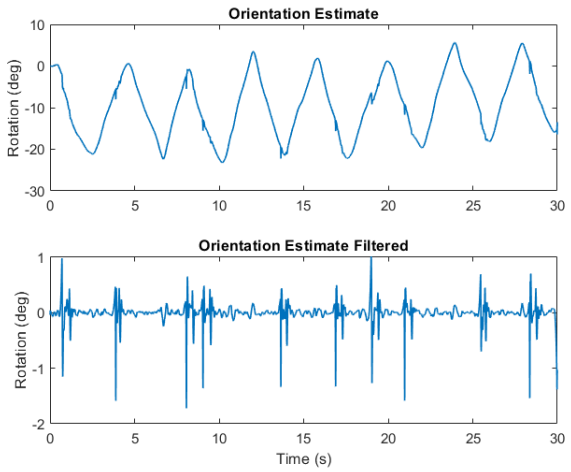

Fig. 10: Example of the orientation data of the move task of one participant. The top graph shows the unfiltered data and the bottom the filtered data in which the perturbation are visible

The distribution of all the recorded deflections is presented in Figure 11. A total of 180 deflections were recorded for the resist and relax tasks, and 120 deflections for the move task. As can be seen, the median deflection for the relax task is the highest at 2.4 degrees, followed by the move task at 2.2 degrees, while the resist task is the lowest at 1.6 degrees.

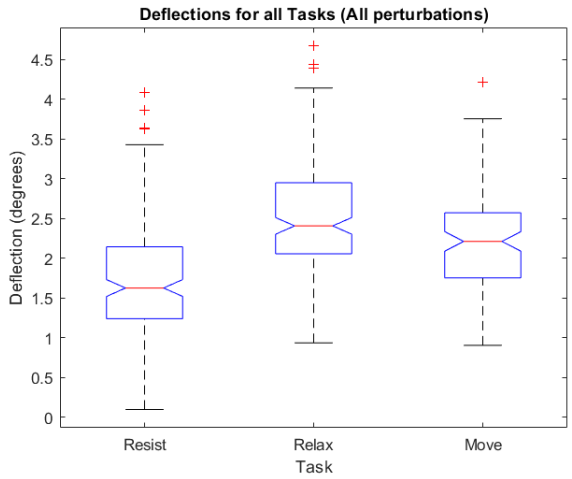

Fig. 11: Distribution of all the deflections of all the participants per task. N=180 deflections were recorded for the resist and relax task and N=110 deflection were recorded for the move task.

B. Additional Experiments

The acceleration of a single perturbation, measured across ten trials (n=10) during the resist task, was recorded and the resulting force was determined, as shown in Figure 12. The solenoid produced a maximum peak force of 7.7 N, with a standard deviation of 0.5 N. The average duration of this force pulse was 30 ms. Considering an average distance from the wrist to the elbow of 29 cm [32] , this force generates a torque of 2.23 Nm.

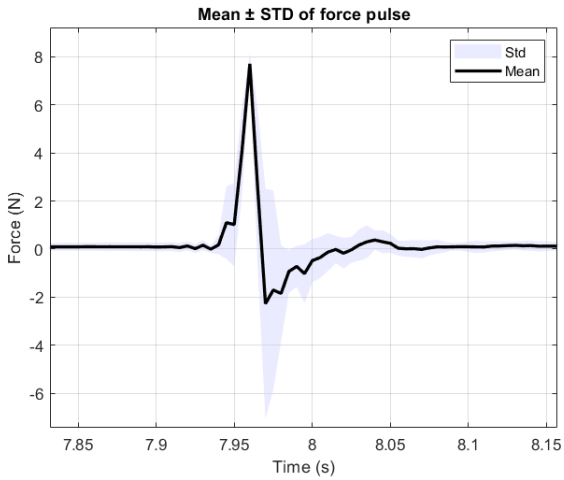

Fig. 12: Mean and standard deviation (n=10) of a single force perturbation given during a resist task.

Experiments to determine the maximum perturbation frequency in different solenoid orientations showed that when the solenoid is in a vertical position with the spring on top, the maximum perturbation frequency is 12 Hz. When turned upside down with the spring at the bottom, the maximum frequency is the lowest at 7 Hz. In the horizontal orientation, the maximum frequency was 11 Hz.

C. Stiffness Estimations

Following the approach by Yagi et al., the stiffness values have been estimated. An overview of these values per task is shown in Fig. 13. The constant α was determined based on the area of the force pulse as seen in Fig. 12, which came down to a constant of 0.78. Due to noise in the measurements, the calculation sometimes gave unrealistic high or negative values. Boundaries have been set up to exclude these values. For the relax and move task these boundaries were 0 and 50 Nm/rad and for the resist task these boundaries were 0 and 120 Nm/rad. Here, the relax task exhibits the lowest average stiffness values, followed by the move task, while the resist task shows the highest values.

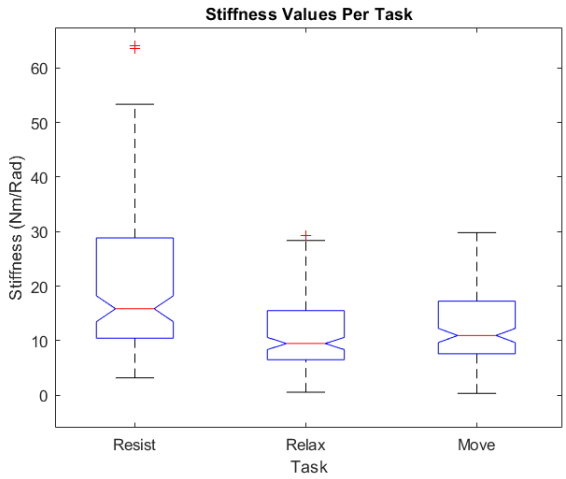

Fig. 13: Box plot with stiffness values per task.

IV. Discussion

The goal of this research experiment was to see whether the prototype could provide ungrounded force perturbations to the underarm that would cause the arm to deflect by approximately 1.7 degrees. We observed that the prototype is capable of generating force perturbations up to 7.7 N, which corresponds to a torque of 2.23 Nm, based on an average wrist-to-elbow distance.

When examining the orientation data from the experiment, perturbations became visible in all three tasks (relax, resist, and move) once sensor drift was filtered out, and movement in the move task was accounted for. The measured average deflections in response to these perturbations exceeded 1.7 degrees for the move and relax tasks and were just under 1.7 degrees for the resist task. The device itself does not restrict the range of motion of the elbow, and its total mass is 325 grams, which is below the 0.5 kg limit set for the prototype.

There are not many ungrounded perturbation devices to compare our device to. Koene et al. did develop a wearable arm perturbator worn on the wrist [33]. This device was capable of delivering force perturbation in two more degrees of freedom and its total mass was lower. Our device however was able to provide slightly more force in one direction, and was tested with human participants.

Another ungrounded arm perturbation device is the one developed by Belden et al. [34]. Their device uses small airjet actuators to generate a perturbation force. With this they were able to give PRBS type perturbations. Our device is not capable of giving such perturbations and compared to their device it is also slightly heavier. However, because of the use of airjets they needed an external high pressure tank which makes it less mobile and the device itself is supposed to be held in the hand which will obstruct from holding objects.

A. Stiffness comparison

The question remains whether the measured deflections are caused purely by the rotation of the elbow joint or if other factors also play a role. When looking at the stiffness values in Fig. 13, the effects of the different tasks are also apparent.

	Relax	**Resist**	**Move**
Estimated stiffness range [Nm/rad]	0-28	3-53	0-30
Estimated stiffness mean values [Nm/rad]	10.46	15.84	13.26
Stiffness ranges found in literature ([22]. [35]) [Nm/rad]	0-10	40-120	4-16

TABLE II: Estimated stiffness values compared to literature

When we compare the average stiffness values with those found in the literature ([22] for the resist and relax tasks and [35] for the move task), we see that the stiffness estimates for the relax and move tasks are slightly higher than expected, whereas the resist task is underestimated (Table II). It is important to note that we cannot directly compare our findings one-to-one with the literature because different methods and estimation techniques have been used. For example, [22] employed a multisine torque perturbation signal, while [35] used a PRBS signal for a differently defined move task. These references nonetheless provide a rough indication of the stiffness ranges we might expect. Several factors can lead to inaccurate stiffness estimation by this device, as discussed below.

1) Connection: The wrist brace used for this prototype can be worn by participants with different arm diameters and lengths, making it versatile in terms of fit. However, this flexibility comes at the cost of a fully rigid connection to the wrist, allowing some of the perturbation energy to be absorbed by the brace rather than fully transferred to

the wrist. Therefore, the actual energy delivered to the wrist could have been lower than intended.

Furthermore, the prototype was attached not only at the wrist but also partly along the forearm. Because the wrist is a bony landmark with relatively little soft tissue, a device attached strictly at the wrist would likely introduce less additional stiffness and damping. In the current setup, however, skin, muscle, and fat tissue along the forearm likely contributed to the measured response, thus misestimating the true stiffness of the arm in all the tasks.

2) Actuator Placement: Another source of potential error comes from the solenoid's off-center positioning below the wrist. While the solenoid generates torque around the flexion/extension direction, its placement also produces torque around the pronation/supination axis of the forearm. Using a mean wrist radius of 21.5 mm [31] and the measured peak force, it is estimated that a peak perturbation torque of around 0.18 Nm about the supination axis occurs. As shown in Fig. 14, this additional torque causes measurable deflection. Because impedance is position-dependent, the extra rotation may interfere with elbow joint parameter estimation, suggesting that the assumption of purely linear system dynamics may not hold under these conditions.

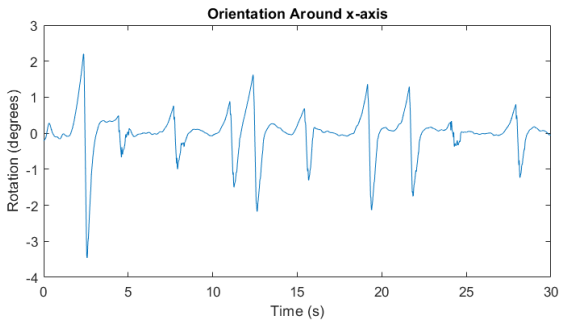

Fig. 14: Example of rotation around the x-axis (pronation wrist) for one participant during the relax task.

Fig. 15 schematically illustrates the different dynamics at play in this setup. Specifically, k_{fa}, b_{fa} represent the flexion/extension stiffness and damping of the arm, while k_{pa}, b_{pa} denote the pronation/supination dynamics. The interface itself contributes additional contact dynamics (k_c, b_c) through skin, muscle, and fat, and the device has its own mechanical stiffness and damping (k_d, b_d). Since these elastic elements can be considered to be arranged in series, the total stiffness is largely dominated by the lowest stiffness in the chain. Consequently, the measured orientation response to the force perturbations may not purely reflect the arm's motion but also includes contributions from soft tissue, the brace, and the off-center actuation of the perturbation device.

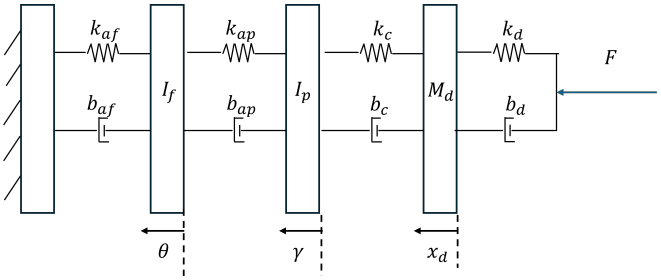

Fig. 15: Schematic mechanical model of the different dynamics involved in the current perturbation setup.

B. Other Limitations of the Device

- **Use of a linear solenoid:** A linear solenoid can apply only short, pulse-type perturbations (see Figure 12), and the width of each pulse cannot be easily controlled. Hence, other perturbation signals (e.g., multisine or PRBS) are not feasible with this actuator. The solenoid can also apply force in only one degree of freedom. To perturb multiple degrees of freedom, multiple solenoids or a rotated configuration would be needed. Furthermore, the maximum contraction frequency of the solenoid changes depending on its orientation, which is an important consideration if the device is not used in a horizontal orientation, which will most likely be the case during ADL.
- **Use of the IMU sensor:** The specific IMU that was used in this setup showed noise over a large frequency range in the orientation data, which made it hard to specifically determine the frequency range of the perturbation response. The sensor choice in a future iteration of the device should be reconsidered.
- **Usage of the Brace:** ADL such as grabbing or holding objects, when wearing the device, is not yet possible in its current configuration. Since the bottom splint in the brace also cover part of the hand this would hinder holding objects.

C. Limitations of the Experiment

- **Participant Selection and Setup:** Since this was a pilot study, the experimental setup was limited to right-handed participants only. Additionally, the holder for the weight-compensation system was attached to the lower arm close to the elbow. This was done to keep the arm in the horizontal plane during the tasks and to prevent fatigue by compensating for the arm's weight as well as keeping the position of the arm for each participant the same. However, fastening the holder below the elbow adds slightly more inertia to the lower arm, which may affect the inertia estimation results.
- **Auditory Distractions:** During the move task, some participants reported difficulty following the metronome beats because the solenoid produced a pronounced clicking sound. For future studies involving an audible cue, it may be preferable to have participants wear headphones to minimize the interference from the solenoid

noise.

D. Future Work

To address the limitations and shortcomings of this device, certain modifications are needed so that it can accurately estimate the impedance parameters of the elbow joint. The primary focus should be on creating a more rigid connection between the device and the wrist—for example, using plaster or a custom 3D-printed cast for each wearer. Secondly, additional rotation around the wrist could be avoided by using a second solenoid on top of the wrist; however, a lighter solenoid may be required to keep the total mass under 0.5 kg. Furthermore, a similar perturbation experiment could be set up in which perturbations cover a wider range of frequencies, allowing the estimation of stiffness, damping, and inertia. A linear time model could then be established to validate these values. Lastly, placing the solenoid in different orientations would allow investigation of the impedance of the arm across multiple degrees of freedom.

V. Conclusion

In this paper, a new design for an ungrounded perturbation device was presented, employing a linear electric actuator. This device is capable of delivering ungrounded force perturbations to the underarm with a maximum peak force of 7.7 N, and it can measure both the input force and the resulting arm dynamics. The system accommodates the full range of motion of the elbow and weighs under 500 grams. An experiment involving human subjects was conducted to evaluate arm deflection in response to these perturbations while participants performed three distinct tasks: relax, resist, and move. The results indicate that the device successfully measured deflections during all tasks. The magnitude of these deflections demonstrated the impact of each task: the relax task produced the largest deflection, followed by the move task, while the resist task showed the smallest deflection. The criteria of an angular arm displacement of 1.7 degrees was met for all tasks except the resist task. Stiffness values were also estimated, but comparisons with the literature revealed some inaccuracies. Consequently, changes in the device's design are required for it to accurately estimate the impedance values of the elbow joint.

VI. Acknowledgments

I would like to give my sincere thanks to my supervisors, Arno Stienen and Jonathan van Zanten, for their guidance, insights and enthusiasm throughout this project. I also wish to thank all the participants for contributing their time to this experiment, as well as everyone in Arno's graduation group for their ongoing support and collaboration. Lastly, I am deeply thankful for the constant encouragement of my family and friends, who have always stood by me.

References

[1] C. F. Prendes *et al.*, "Burden of stroke in europe: An analysis of the global burden of disease study findings from 2010 to 2019," *Stroke*, vol. 55, no. 2, pp. 432–442, 2024. DOI: 10.1161/STROKEAHA.122.042022.

[2] M. C. Emos and S. Agarwal, "Neuroanatomy, upper motor neuron lesion," in *StatPearls [Internet]*, Updated 2023 Aug 14. Available from: https://www.ncbi.nlm.nih.gov/books/NBK537305/, Treasure Island, FL: StatPearls Publishing, 2025.

[3] K. M. Zackowski *et al.*, "How do strength, sensation, spasticity and joint individuation relate to the reaching deficits of people with chronic hemiparesis?" *Brain*, vol. 127, no. 5, pp. 1035–1046, 2004, ISSN: 0006-8950. DOI: 10.1093/brain/awh116. [Online]. Available: https://doi.org/10.1093/brain/awh116.

[4] A. Harb and S. Kishner, "Modified ashworth scale," in *StatPearls*. Treasure Island (FL): StatPearls Publishing Copyright © 2024, StatPearls Publishing LLC., 2024, Harb, Andrew Kishner, Stephen Study Guide Book Chapter Disclosure: Andrew Harb declares no relevant financial relationships with ineligible companies. Disclosure: Stephen Kishner declares no relevant financial relationships with ineligible companies. NBK554572 [bookaccession].

[5] S. Morris, "Ashworth and tardieu scales: Their clinical relevance for measuring spasticity in adult and paediatric neurological populations," *Physical Therapy Reviews*, vol. 7, no. 1, pp. 53–62, 2002, doi: 10.1179/108331902125001770, ISSN: 1083-3196. DOI: 10.1179/108331902125001770. [Online]. Available: https://doi.org/10.1179/108331902125001770.

[6] E. Zurawski *et al.*, "Interrater reliability of the modified ashworth scale with standardized movement speeds: A pilot study," *Physiother Can*, vol. 71, no. 4, pp. 348–354, 2019, 1708-8313 Zurawski, Erica Behm, Kirsten Dunlap, Charlotte Koo, James Ismail, Farooq Boulias, Chris Reid, Shannon Phadke, Chetan P Journal Article Canada 2019/11/26 Physiother Can. 2019 Fall;71(4):348-354. doi: 10.3138/ptc-2018-0086., ISSN: 0300-0508 (Print) 0300-0508. DOI: 10.3138/ptc-2018-0086.

[7] F. Li, Y. Wu, and X. Li, "Test-retest reliability and inter-rater reliability of the modified tardieu scale and the modified ashworth scale in hemiplegic patients with stroke," *Eur J Phys Rehabil Med*, vol. 50, no. 1, pp. 9–15, 2014, 1973-9095 Li, F Wu, Y Li, X Journal Article Italy 2013/12/07 Eur J Phys Rehabil Med. 2014 Feb;50(1):9-15. Epub 2013 Dec 5., ISSN: 1973-9087.

[8] P. Raghavan, "Upper limb motor impairment after stroke," *Physical Medicine and Rehabilitation Clinics of North America*, vol. 26, no. 4, pp. 599–610, 2015, Stroke Rehabilitation, ISSN: 1047-9651. DOI: https://doi.org/10.1016/j.pmr.2015.06.008. [Online]. Available: https://www.sciencedirect.com/science/article/pii/S1047965115000558.

[9] J. H. Morris *et al.*, "Predicting health related quality of life 6 months after stroke: The role of anxiety and upper limb dysfunction," *Disability and Rehabilitation*, vol. 35, no. 4, pp. 291–299, 2013, doi: 10.3109/09638288.2012.691942, ISSN: 0963-8288. DOI: 10.3109/09638288.2012.691942. [Online]. Available: https://doi.org/10.3109/09638288.2012.691942.

[10] R. Kearney and I. Hunter, "System identification of human joint dynamics," *Critical reviews in biomedical engineering*, vol. 18, pp. 55–87, Feb. 1990.

[11] K. ter Welle, *Identification of intrinsic and reflexive joint impedance*, 2024.

[12] M.-S. Ju *et al.*, "Time-course analysis of stretch reflexes in hemiparetic subjects using an on-line spasticity measurement system," *Journal of Electromyography and Kinesiology*, vol. 10, no. 1, pp. 1–14, 2000, ISSN: 1050-6411. DOI: https://doi.org/10.1016/S1050-6411(99)00018-8. [Online]. Available: https://www.sciencedirect.com/science/article/pii/S1050641199000188.

[13] A. J. Starsky *et al.*, "Reliability of biomechanical spasticity measurements at the elbow of people poststroke," *Archives of Physical Medicine and Rehabilitation*, vol. 86, no. 8, pp. 1648–1654, 2005, ISSN: 0003-9993. DOI: https://doi.org/10.1016/j.apmr.2005.03.015. [Online]. Available: https://www.sciencedirect.com/science/article/pii/S0003999305003217.

[14] C. G. Meskers *et al.*, "Neurocontrol of movement: System identification approach for clinical benefit," *Frontiers in Integrative Neuroscience*, vol. 9, 2015, ISSN: 1662-5145. DOI: 10.3389/fnint.2015.00048. [Online]. Available: https://www.frontiersin.org/journals/integrative-neuroscience/articles/10.3389/fnint.2015.00048.

[15] F. C. T. van der Helm *et al.*, "Identification of intrinsic and reflexive components of human arm dynamics during postural control," *Journal of Neuroscience Methods*, vol. 119, no. 1, pp. 1–14, 2002, ISSN: 0165-0270. DOI: https://doi.org/10.1016/S0165-0270(02)00147-4. [Online]. Available: https://www.sciencedirect.com/science/article/pii/S0165027002001474.

[16] R. E. Kearney, R. B. Stein, and L. Parameswaran, "Identification of intrinsic and reflex contributions to human ankle stiffness dynamics," *IEEE Transactions on Biomedical Engineering*, vol. 44, no. 6, pp. 493–504, 1997, ISSN: 1558-2531. DOI: 10.1109/10.581944.

[17] L. Galiana, J. Fung, and R. Kearney, "Identification of intrinsic and reflex ankle stiffness components in stroke patients," *Exp Brain Res*, vol. 165, no. 4, pp. 422–34, 2005, Galiana, Laura Fung, Joyce Kearney, Robert Journal Article Research Support, Non-U.S. Gov't Germany 2005/07/02 Exp Brain Res. 2005 Sep;165(4):422-34. doi: 10.1007/s00221-005-2320-z. Epub 2005 Jul 1., ISSN: 0014-4819 (Print) 0014-4819. DOI: 10.1007/s00221-005-2320-z.

[18] L. L. van der Velden *et al.*, "Development of a single device to quantify motor impairments of the elbow: Proof of concept," *Journal of NeuroEngineering and Rehabilitation*, vol. 19, no. 1, p. 77, 2022, ISSN: 1743-0003. DOI: 10.1186/s12984-022-01050-2. [Online]. Available: https://doi.org/10.1186/s12984-022-01050-2.

[19] R. Happee, E. Vlugt, and A. Schouten, "Posture maintenance of the human upper extremity; identification of intrinsic and reflex based contributions," *SAE International Journal of Passenger Cars - Mechanical Systems*, vol. 1, pp. 1125–1135, 2008. DOI: 10.4271/2008-01-1888.

[20] H. M. Hondori and A. W. Tech, "Smart mug to measure hand's geometrical mechanical impedance," in *2011 Annual International Conference of the IEEE Engineering in Medicine and Biology Society*, 2011, pp. 4053–4056. DOI: 10.1109/IEMBS.2011.6091007.

[21] P. L. Weiss, R. E. Kearney, and I. W. Hunter, "Position dependence of ankle joint dynamics–ii. active mechanics," *J Biomech*, vol. 19, no. 9, pp. 737–51, 1986, Weiss, P L Kearney, R E Hunter, I W Journal Article Research Support, Non-U.S. Gov't United States 1986/01/01 J Biomech. 1986;19(9):737-51. doi: 10.1016/0021-9290(86)90197-1., ISSN: 0021-9290 (Print) 0021-9290. DOI: 10.1016/0021-9290(86)90197-1.

[22] M. van de Ruit *et al.*, "System identification: A feasible, reliable and valid way to quantify upper limb motor impairments," *Journal of NeuroEngineering and Rehabilitation*, vol. 20, no. 1, p. 67, 2023, ISSN: 1743-0003. DOI: 10.1186/s12984-023-01192-x. [Online]. Available: https://doi.org/10.1186/s12984-023-01192-x.

[23] M. M. Mirbagheri *et al.*, "Neuromuscular abnormalities associated with spasticity of upper extremity muscles in hemiparetic stroke," *Journal of Neurophysiology*, vol. 98, no. 2, pp. 629–637, 2007, doi: 10.1152/jn.00049.2007, ISSN: 0022-3077. DOI: 10.1152/jn.00049.2007. [Online]. Available: https://doi.org/10.1152/jn.00049.2007.

[24] N. Doup, "Actuation mechanisms for an ungrounded force-feedback device for arm impedance measurements: A systematic review," 2024.

[25] A. L. Pando *et al.*, "Position-dependent characterization of passive wrist stiffness," *IEEE Transactions on Biomedical Engineering*, vol. 61, no. 8, pp. 2235–2244, 2014. DOI: 10.1109/TBME.2014.2313532.

[26] J. Andersen and T. Sinkjaer, "An actuator system for investigating electrophysiological and biomechanical features around the human ankle joint during gait," *Rehabilitation Engineering, IEEE Transactions on*, vol. 3, pp. 299–306, Jan. 1996. DOI: 10.1109/86.481969.

[27] M. Vlaar and A. Schouten, "System identification for human motion control," vol. 2015, Jul. 2015, pp. 600–605. DOI: 10.1109/I2MTC.2015.7151336.

[28] K. Yagi, K. Suzuki, and H. Mochiyama, "Human joint impedance estimation with a new wearable device utilizing snap-through buckling of closed-elastica," *IEEE Robotics and Automation Letters*, vol. 3, pp. 1506–1513, 2018. DOI: 10.1109/LRA.2018.2800114.

[29] K. Yagi and H. Mochiyama, "Human wrist impedance estimation based on impulse response induced by snap-through buckling of closed-elastica," in *2019 41st Annual International Conference of the IEEE Engineering in Medicine and Biology Society (EMBC)*, 2019, pp. 5339–5343, ISBN: 1558-4615. DOI: 10.1109/EMBC.2019.8857383.

[30] K. Yagi and H. Mochiyama, "On the determination of mapping rule and sampling interval for human joint impedance estimation," in *2017 56th Annual Conference of the Society of Instrument and Control Engineers of Japan (SICE)*, 2017, pp. 1357–1362. DOI: 10.23919/SICE.2017.8105737.

[31] K. Reckelhoff *et al.*, "Ultrasound evaluation of the normal ulnar nerve in guyon's tunnel: Cross-sectional area and anthropometric measurements," *Journal of Medical Ultrasound*, vol. 23, Oct. 2015. DOI: 10.1016/j.jmu.2015.09.002.

[32] C. Gordon *et al.*, "Anthropometric survey of u.s. army personnel: Summary statistics, interim report for 1988," Jan. 1989.

[33] R. Koene, "Design and validation of ungrounded wrist perturbator based on parallel mechanism," unpublished, M.S. thesis, Delft University of Technology, 2022.

[34] J. Belden *et al.*, "A portable air jet actuator device for mechanical system identification," *Review of Scientific Instruments*, vol. 82, no. 3, p. 035 106, 2011, ISSN: 0034-6748. DOI: 10.1063/1.3562894. [Online]. Available: https://doi.org/10.1063/1.3562894.

[35] D. J. Bennett *et al.*, "Time-varying stiffness of human elbow joint during cyclic voluntary movement," *Experimental Brain Research*, vol. 88, no. 2, pp. 433–442, 1992, ISSN: 1432-1106. DOI: 10.1007/BF02259118. [Online]. Available: https://doi.org/10.1007/BF02259118.

[36] J. Veneman *et al.*, "A series elastic- and bowden-cable-based actuation system for use as torque actuator in exoskeleton-type robots.," *I. J. Robotic Res.*, vol. 25, pp. 261–281, Jan. 2006.

APPENDIX I
CONCEPTUALIZATION

To investigate mechanisms capable of generating ungrounded forces and to consolidate findings from the literature, an overview was created using the ACCREx tree format, as shown in Fig. 16. Most mechanisms identified in the literature rely on principles that can be categorized into three main groups: Linear Moving Mass, Angular Moving Mass, and Air Propulsion.

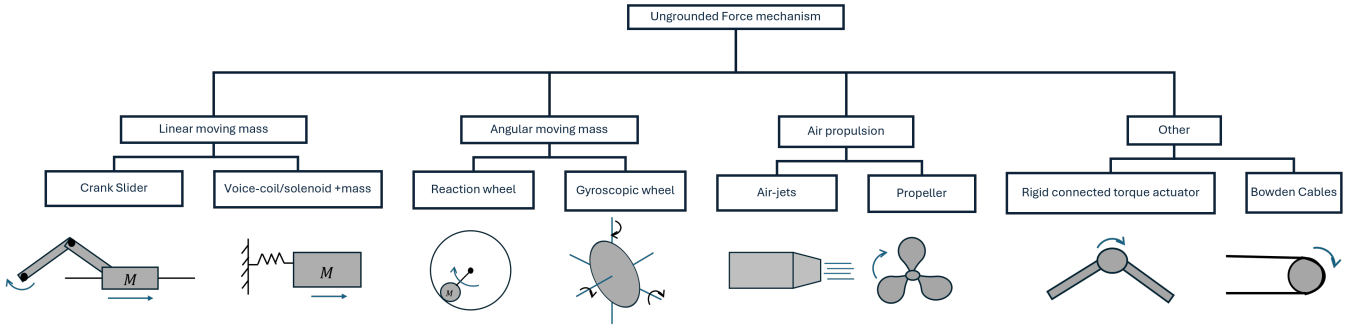

Fig. 16: ACCREx tree with possible mechanical solution for generating a ungrounded force perturbation

A concept of an ungrounded perturbator should adhere to to the following criteria:

- The device should be able to give ungrounded force perturbations to the underarm.
- The force perturbations must be larger than 4N.
- The device should allow full range of motion of the elbow (140 degrees from fully flexed to fully extended position).
- The device must not be heavier than 0.5 kg.
- The device must be able to measure the acceleration of the forearm.
- The device must not be invasive.
- The length of the device must not be larger 29 centimeters (average distance of the wrist to the elbow) [32].
- The device should incorporate a safety mechanism.
- The device should be comfortable to wear for the duration of typical impedance estimation experiments.

To narrow down these mechanisms, they were evaluated against four additional weighted performance criteria, as summarized in Table III.

1) Added Mass: The weight of the device is critical as increased mass can hinder daily activities and reduce user comfort. Additionally, added mass complicates measurements by requiring greater acceleration for perturbation.
2) Intrusiveness: This criterion considers the extent to which the device restricts freedom of movement or obstructs activities of daily living. Devices with lower bulk and greater mobility are more desirable.
3) Number of Parts: A mechanism with fewer components is preferable, as it simplifies manufacturing, reduces potential errors, and decreases assembly complexity.
4) Number of Part available: Mechanisms that rely on readily available parts are favored over those requiring custom manufacturing, as the latter increases the risk of errors and prolongs prototyping.

Since the first two criteria are more important for the user their weight is higher than the last two. After evaluating the mechanisms, the top three scoring solutions were:

- Linear Electric Actuator
- Bowden Cable Mechanism
- Direct Torque Actuator on the Elbow

These mechanisms stood out primarily due to their compact design and minimal weight addition, making them well-suited for practical application without significantly affecting arm mobility or user comfort.

		Voice coil/solenoid		Torque motor		Linear motor		Rotating mass		Air-jets		Bowden cable	
	weight	score	weighted	score	weighted	score	weighted	score	weighted	score	weighted	score	weighted
Mass	2	4	8	2	4	2	4	2	4	5	6	5	10
Intrusiveness	2	4	8	3	6	2	4	3	6	4	6	2	4
Number of parts available	1	4	4	5	5	4	4	3	3	2	2	4	4
Number of parts	1	2	2	4	4	4	4	3	3	2	2	4	4
Total			**20**		**19**		**16**		**16**		**16**		**22**

TABLE III: Mechanisms compared based on weighted criteria

A. *Power Calculations*

Before selecting one of the three highest-scoring mechanisms, it is crucial to evaluate the power requirements of each to determine their feasibility for an arm-worn solution. Models were developed for each mechanism to calculate and visualize power usage and dynamics. These models assume the elbow joint as a second-order system described by:

$$T = I\ddot{\theta} + b\dot{\theta} + k\theta \tag{7}$$

Here, T represents the applied perturbation torque, and I, b, and k correspond to the arm's inertia, elbow joint rotational damping, and rotational stiffness, respectively. These values, derived from measurements at 10% maximum voluntary contraction (as reported in [11]), are $I = 0.11kg * m^2, b = 1.4Nm * s/rad$ and $k = 22Nm/rad$. This contraction level approximates scenarios encountered during activities of daily living (ADL).

The input force or torque for each mechanism was iteratively adjusted to achieve a minimum arm deflection of 2 degrees.

1) Torque motor: For the torque motor a rigid connection was assumed and a simplified model of this can be seen in Fig. 17a. A torque perturbation of 0.84 Nm for 0.5 seconds was the input for this model. It shows that the maximum power needed for this single perturbation would be around 0.26 W

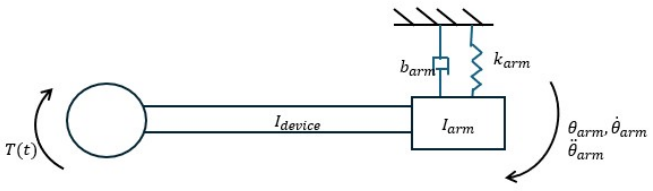

(a) visual simplified model of torque mechanism

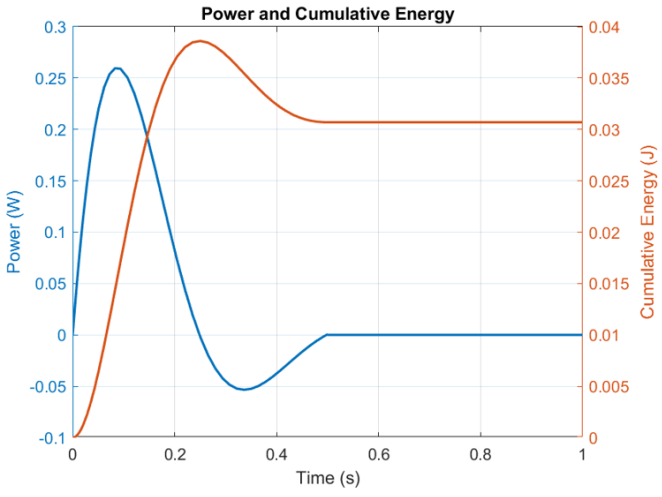

(b) Power torque motor

Fig. 17: Model of the torque actuator mechanism

2) Bowden cables: Fig. 18 show the model of the Bowden cable mechanism. The cables are modeled as stiff springs with a stiffness of $k_i = 648kN, k_o = 2428kN$ for the stiffness of the inner cable and the outer sheet respectively. There is also an extra spring in series with these cables with a stiffness of $k_{se} = 4kN$ which allows for better force control and is more shock resistant [36]. It can be seen that the maximum power is higher, around 0.64 W, for a torque perturbation of 1.7 Nm for 0.5 seconds. This is mainly because of the loss of energy in the cables due to friction.

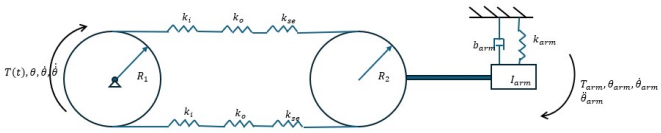

(a) visual simplified model of the cable mechanism

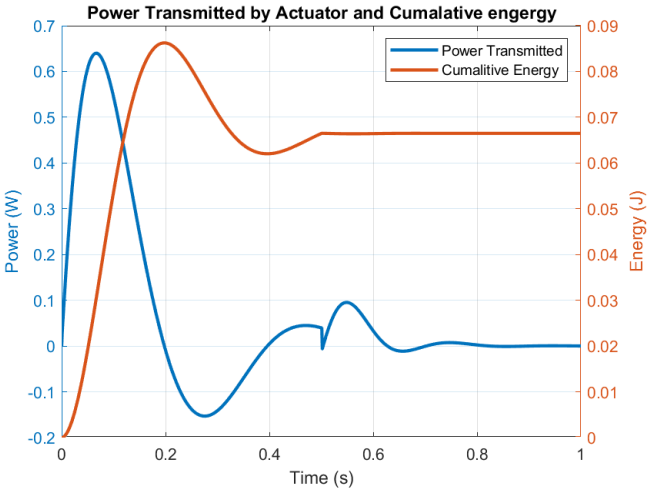

(b) Power cable model

Fig. 18: Model of the Bowden cable mechanism

3) Linear actuator: The linear actuator mechanism is simplified to a shooting mass connected to a spring (like in a solenoid or voice-coil actuator) that collides with an enclosure with a certain stiffness and damping ($k_c = 500kN/m$, $b_c = 100Ns/m$). The acceleration and collision will create a reaction force on the arm causing it to deflect. As the mass moves it is also experiencing the stiffness of the spring ($k_1 = 14N/m$) and damping due to friction ($b_1 = 1.4Ns/m$). As Fig. 19b shows this mechanism requires the highest power of 26W for a deflection of around 2 degrees of the arm.

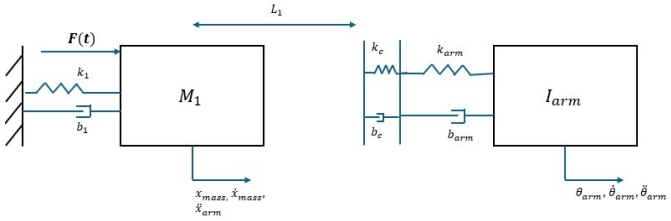

(a) visual simplified model of the shooting mass mechanism

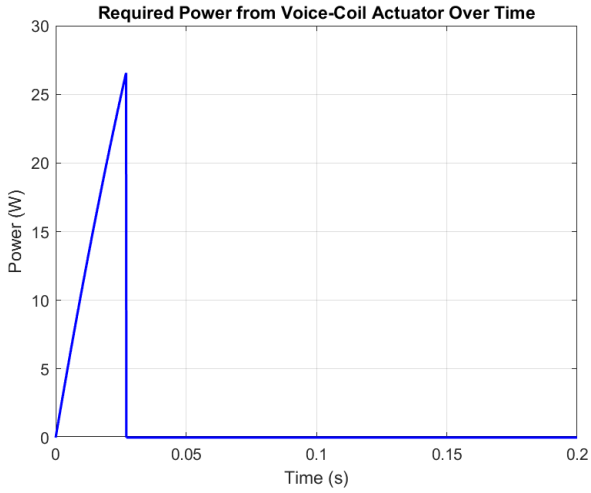

(b) Power shooting mass model

Fig. 19: Model of the Bowden cable mechanism

APPENDIX II
ACTUATOR CHOICE

To choose the best solenoid actuator that could be used for the prototype, multiple solenoids have been compared with each other. To speed up the prototyping process and to minimize the costs only solenoids that were ready available and under 40 euros were considered shown in table IV. These were often hobby type actuators for amateur usage. Since it is important for the solenoid to provide a high force perturbation while also being lightweight and compact, the solenoids are compared with each other based on power density based on mass and volume and their force density based on mass and volume. Table V shows that the best performing solenoid based on these criteria is the WANGCL FJ-Z05.

TABLE IV: Specifications of various considered solenoid actuator

	Stroke (mm)	**Max force (N)**	**Voltage (V)**	**Current (A)**	**Power (W)**	**Volume (cm$\hat{3}$)**	**Mass (g)**
HS-1564B	25	30	12	3.0	36.0	72.96	370
HS-1040B	10	25	12	1.6	19.2	28.32	140
Wangcl FJ-Z05	15	45	12	2.5	30.0	37.50	190
HS-1250	10	60	12	3.7	44.4	79.92	350

TABLE V: Solenoids compared to each other based on force and power performance relative to their mass and volume

	Force density (volume)	**Power density (volume)**	**Force density (mass)**	**Power densitiy (mass)**	**Mass (g)**
HS-1564B	0,41	0,49	0,08	0,10	370
HS-1040B	0,88	0,68	0,18	0,14	140
Wangcl FJ-Z05	1,20	0,80	0,24	0,16	190
HS-1250	0,75	0,56	0,17	0,13	350

APPENDIX III
ELECTRICAL WIRING OF THE PROTOTYPE

Below the electrical wiring of the micro controller (Seeeduino Nano), solenoid, sensors and adjustable power supply can be seen. The micro controller is connected to and powered by the laptop. The SCL clock line and the SDA data line of the ADXL345 sensor and MPU6050 IMU sensor are connected the pins A5 and A4, respectively. These pins on the micro controller are designated for its I2C connection which is used by the sensors. The Vcc line of the sensors is connected to the 5V supply on the Arduino. the motor is connected by the external adjustable power supply because the controller itself can not deliver enough power. It is placed in series with a flyback diode (IN5822) to prevent current flowing in opposite direction when the solenoid is turned off. The D6 pin is connected to a MOSFET transistor (IRLZ44N N channel MOSFET) that regulates the current through the solenoid: it closes the circuit when the pin is set to high and breaks the circuit when set to low. Between the D6 line and the ground of the transistor an 100Ω pull-up resistor was used to ensure the signal was strong enough to activate the transistor when the pin is set to high and a 1kΩ pull-down resistor is placed between the pin and the ground to ensure the signal is 0 when the pin is set to low. Between the solenoid and the power supply the emergency button is placed that will break the circuit when pressed.

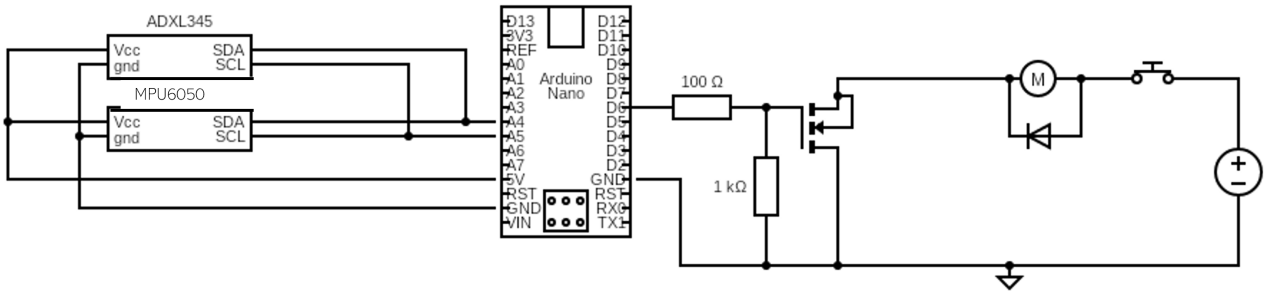

Fig. 20: Electrical wiring

APPENDIX IV
EXPERIMENTAL PROTOCOL

A. Preparing the experiment

Before starting the experimental procedure, the following steps must be taken to ensure the participant's safety and understanding of the experiment:

- Start up the laptop and open the MATLAB file for the experiment.
- Check if the acceleration sensors are functioning correctly and providing output.
- Provide the participant with detailed instructions about the experiment, including its purpose, tasks, and duration (through the informed concent form). Allow them to ask questions to ensure clarity.
- Make sure the participants is seated with their back against the seat of the chair and the legs of the chair are placed on the marking on the floor.
- Securely attach the wearable perturbator to the participant's dominant arm; operator ensures a tight fit.
- The underarm of the participant is placed in the holder of the SaeboMas mini in a way that the medial head of the epicondyle of the participant is aligned with the end of the holder.
- Ask the participant to move their arm to the line marked on the desk and align their arm with the line.
- Ask the participant to fully relax their arm and see if their arm makes contact with the desk. If so, increase the force of the SaeboMas mini until there is no contact anymore.
- The stop button is placed within reach of the participants non-dominant arm and within reach of the researcher.
- The power source of the perturbation device is being put on.
- Conduct a trial run to familiarize the participant with the perturbation strength and with the task they need to perform.

B. Start of the experiment

The main experimental procedure involves the following steps:

- Assign an anonymous identifier to the name of the data file that will be saved when the task is completed.
- Load the correct pulse file for the experiment.
- Instruct the participant to fully relax their arm for 30 seconds and actively resist the applied random perturbations.
- Ask if the participant is ready and then start the experiment by running the data collection section in the script.
- After the perturbations are completed, ensure the data file is correctly saved in the designated directory.
- Repeat the task and data collection for a second time. Save under a different name.
- Start second part of the experiment: The resist task
- Provide instructions for the second task: The participant should flex their arm and resist all perturbation
- Load the correct pulse file and collect the data like before.
- Perform this task twice.
- Start the third part of the experiment: The move task.
- Provide instructions for the third task: the participant should move their arm from left to right to the markings on the desk on the beat of the metronome that is being played from a phone.
- Before the task starts the participant should move their arm to the left marking which is the starting point for this task.

- Set up the metronome on the phone.
- Load the third pulse signal.
- Run the data collection section and tell the participant to start moving when a count of the metronome is heard to properly synchronize.
- Save the data file and repeat the task for a second time

C. End of the experiment

The final steps of the protocol are as follows:

- Carefully remove the brace from the participant or allow them to do so. Avoid contact with the blue coil of the solenoid, as it may be hot.
- Leave the brace unused and for at least 30 minutes before starting a next experiment with a new participant to allow it to cool down.

APPENDIX V
DEVICE REPORT

Delft University of Technology
INSPECTION REPORT FOR DEVICES TO BE USED IN CONNECTION WITH HUMAN SUBJECT RESEARCH

This report should be completed for every experimental device that is to be used in interaction with humans and that is not CE certified or used in a setting where the CE certification no longer applies[1].

The first part of the report has to be completed by the researcher and/or a responsible technician.

Then, the safety officer (Heath, Security and Environment advisor) of the faculty responsible for the device has to inspect the device and fill in the second part of this form. An actual list of safety-officers is provided on this webpage.

Note that in addition to this, all experiments that involve human subjects have to be approved by the Human Research Ethics Committee of TU Delft. Information on ethics topics, including the application process, is provided on the HREC website.

Device identification (name, location): Wearable perturbator located in the Robotlab, room 34-E-K-180 at the ME faculty.

Configurations inspected[2]: NA

Type of experiment to be carried out on the device:[3] Human experiments that involve small perturbations of the arm.

Name(s) of applicants(s): Arno Stienen

Job title(s) of applicants(s): Associate Professor BmechE

(Please note that the inspection report should be filled in by a TU Delft employee. In case of a BSc/MSc thesis project, the responsible supervisor has to fill in and sign the inspection report.)

Date: 11/12/2024

Signature(s): 

1 Modified, altered, used for a purpose not reasonably foreseen in the CE certification

2 If the devices can be used in multiple configurations, otherwise insert NA

3 e.g. driving, flying, VR navigation, physical exercise, ...

Setup summary

The wearable perturbator (figure 1-3) is a device that can give ungrounded force perturbation to the underarm. The device consists of a wrist brace with an electrical solenoid motor and multiple accelerometers (ADXL345) attached to it. One accelerometer is attached to the brace itself to measure the acceleration of the participants arm in response to the force perturbation. The other is attached to the body of the solenoid to measure the acceleration of the moving mass and thereby the applied perturbation force. All of the acceleration data will be processed in Matlab.

The solenoid generates a force by accelerating and decelerating its own mass. It is driven by an Arduino nano and the whole system is powered by an external adjustable power supply. In case of any emergency there is also an emergency button that either the participant or the researcher can press which cuts off the power supply and thus stopping the solenoid. The power supply is also within reach of the researcher and can be switched off at any time. The full electrical wiring diagram can be seen in Appendix 1.

For the experimental setup the participant is placed on a desk chair the brace is tightly put on the participants dominant arm. This experiment is only focused on the elbow joint and the mass of the lower arm so to compensate for the weight of the upper arm it is placed in an arm holder.

The experiment will consist of two parts: for the first part the participant has to fully flex their arm and resist the perturbation. For the second part the participant has to fully relax their arm and try not to interact with the applied perturbations. For each part four different perturbation frequency are applied to the arm.

The experiment with the wearable perturbator will only involve healthy participants.

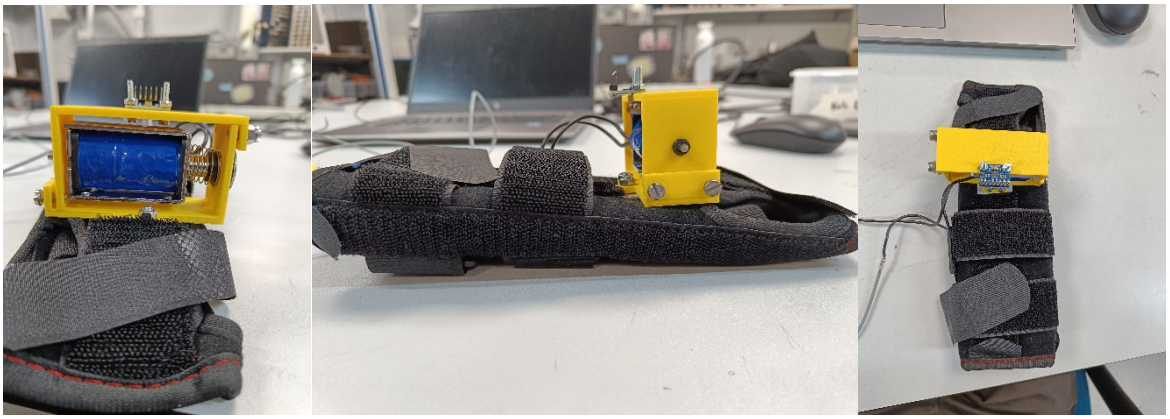

Figure 1-3: Side and top view of the device.

Risk checklist

Please fill in the following checklist and consider these hazards that are typically present in many research setups. If a hazard is present, please describe how it is dealt with.

Also, mention any other hazards that are present.

Hazard type	Present	Hazard source	Mitigation measures
Mechanical (sharp edges, moving equipment, etc.)	X	The splint that is inside the brace could cause discomfort while the device is active.	A physical stop button is within reach of the participant so they could press it when they feel uncomfortable.
Mechanical (sharp edges, moving equipment, etc.)	X	The splints in the brace can cause discomfort when it is fastened too tightly.	The participant fastens the brace themselves on their arm so they can adjust it themselves to prevent discomfort.
Electrical	X	Due to electrical malfunction the device could stay on for too long or run out of control.	There are virtual safety stops programmed that engage when the solenoid actuation extends the experiment time. If these virtual stops fail the physical stop button can be pressed to complete cut of the electrical circuit.
Structural failure	X	Due to high velocity the connection of the solenoid and the brace might break causing the solenoid to fall on the participant.	The arm of the participant is placed next to the body and above a desk so if the solenoid detaches from the brace it does not fall on the body or feet of the participant.
Touch Temperature	X	When the solenoid actuator is turned on for too long (beyond the maximum experiment time) the coil could get hot.	Two experiments are never conducted right after each other but there is a rest time of at least 30 minutes to prevent overheating the solenoid motor. The Power source is always switched off after each experiment.
Electromagnetic radiation	-		
Ionizing radiation	-		
(Near-)optical radiation (lasers, IR-, UV-, bright visible light sources)	-		
Noise exposure	-		
Materials (flammability, offgassing, etc.)	-		
Chemical processes	-		
Fall risk	-		

Device inspection

(to be filled in by the AMA advisor of the corresponding faculty)

Name: Maarten Lugt

Faculty: Mechanical Engineering

The device and its surroundings described above have been inspected. During this inspection I could not detect any extraordinary risks.

(Briefly describe what components have been inspected and to what extent (i.e. visually, mechanical testing, measurements for electrical safety etc.)

The perpetubator has been shown to me. no additional risks other than described are expected.

Date: 06-01-2025

Signature: 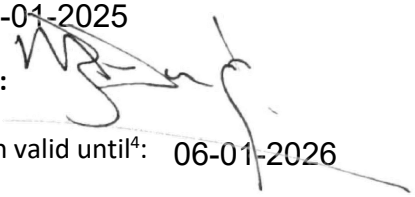

Inspection valid until[4]: 06-01-2026

Note: changes to the device or set-up, or use of the device for an experiment type that it was not inspected for require a renewed inspection

4 Indicate validity of the inspection, with a maximum of 3 years

APPENDIX VI
INFORMATION FOR PARTICIPANT

Dear Participant,

You are invited to take part in a study called **"Validation of a Wearable Perturbation Device"**. This research is being conducted by Niels Doup (Master's student in Mechanical Engineering) under the supervision of Arno Stienen (Assistant Professor, BMechE department, TU Delft) and Jonathan van Zanten (PhD candidate, BMechE department, TU Delft).

Purpose of the Study

In research, perturbation devices are used to determine the impedance of specific joints. Joint impedance generally describes the resistance of a joint in response to an external perturbation. When people that have damage to certain nerves in their upper body, caused by a stroke for example, it can affect the stiffness of their joint and the reflex response to joint movement.

The purpose of this study is to test the functionality of a new wearable perturbation device. This device will apply ungrounded force perturbations to the forearm. The speed, acceleration, and position of the forearm in response to these perturbations will be measured.

The study consists of two parts:

1. In the first part, you will be asked to fully tense your arm and resist all applied perturbations.
2. In the second part, you will be asked to move your arm from left to right and back again between two markings on the desk, synchronized with a metronome.

In each part, perturbations at a random interval will be applied, each lasting 30 seconds. The complete experiment will take approximately 30 minutes. This study only focusses on the effect of the perturbation on the lower arm and elbow joint. Therefore before the experiment starts the upper arm is placed in a holder to compensate for its weight.

<u>What data will be acquired and what will happen to it?</u>

During both parts of the experiment the position, acceleration data of the underarm will be collected and saved as well as the acceleration data of the moving mass that is attached to the arm. This data will be used to validate the concept and see if the concept is able to determine the joints impedance response to the perturbations.

Your data will be anonymized with a unique number, thereby dissociating the data from directly identifiable information such as your name. After one week, the document linking your kinematic data to your name will be deleted. The data will be used for research that may result in publication of a master's thesis.

To reduce the possibility that your age and gender lead to your re-identification, your exact age will not be stored. Instead, you will be assigned to an 'age-group' (e.g. 18-25, 25-35 etc.). Your age group and gender will be stored together with the kinematic data of the underarm for further research.

<u>What are the risks associated with this study?</u>

The device can give force perturbation to the under arm but these are not large enough cause overstretching to the joint or do any harm. However, if in any case during the experiment you feel unwell or the device heats up too much there are several safety mechanisms built in:

- A virtual time limit: the device automatically shuts off when it is activated for too long
- A physical safety button in reach of you and the researchers that you can press at all times during the experiment. This will result in the device being immediately shut down.

Appendix VII
Concent Form

For participation in the study: '*Validation of a wearable perturbation device'* **Please check the appropriate box**

Participation in the study	*Yes*	*No*
I have read and understood the participant information from 01/2025. I have asked my questions about the study, and they have been answered to my satisfaction.		
I voluntarily consent to participate in this study as a participant, and I understand that I can refuse to answer questions and that I can withdraw from the study at any time without giving a reason.		
I understand that there is no compensation for my participation.		
I understand that participation in the study involves undergoing force perturbation applied to the forearm and kinematic measurements (acceleration of the forearm)		
I understand that taking part in the study involves the following risks, as described in the participant information, namely: - Device overheating I understand that these will be mitigated by numerous safety mechanisms present as described in the participant information, namely: - Virtual end-stops for the device based on time powered on. - Cool down time between two experiments. - An emergency button within reach of both participant and researcher.		
I understand that the following steps will be taken to minimize the threat of a data breach, and protect my identity in the event of such a breach: - Anonymization of data through using a 'key' linked to my data, instead of my name. The link between 'key' and name is removed one week after data collection. - Storing all information, and the link between the 'key' and my name, on a secured project drive, instead of locally on a laptop.		
I understand that taking part in the study also involves collecting specific personally identifiable information (PII), specifically my name, sex, and age, with the potential risk of my identity being revealed.		
I understand that the personal information that can identify me, like my name and age, will not be shared outside the study team.		
I give permission to the research team to archive all data (age, gender, kinetic measurements) that has been collected from me, to use for future research and learning.		

_____ _____ _____

Name of participant Signature Date

I, as researcher, have accurately read out the information sheet to the potential participant and, to the best of my ability, ensured that the participant understands to what they are freely consenting.

_____ _____ _____

Researcher name Signature Date

APPENDIX VIII
DATA COLLECTION

```
clear
close all
clc
%% Initialization
% Ensure the Arduino Support Package is installed
% Create an Arduino object
arduinoObj = arduino('COM8', 'Nano3', Libraries='I2C');
sensor1 = adxl345(arduinoObj, "I2CAddress", 0x53, SampleRate=200, SamplesPerRead=10,
    ReadMode="latest", OutputFormat="matrix", TimeFormat="duration"); % ADXL345
   sensor
sensor2 = mpu6050(arduinoObj, SampleRate=200, SamplesPerRead=10, ReadMode="latest",
   OutputFormat="matrix", TimeFormat="duration"); % MPU6050 sensor

% Define parameters
pulsePin = 'D6';          % Digital pin for pulse output
%% Load Pulse Signal
load("randomPulseSignal_trial.mat");
%%
% Calibration Phase
calibrationDuration = 2; % Calibration duration in seconds
calibrationData1 = [];
calibrationAccel2 = [];
calibrationGyro2 = [];
disp('Calibrating sensors...');

calibrationStartTime = tic;
while toc(calibrationStartTime) < calibrationDuration
    % Read sensor data during calibration
    [sensorReadings1, ~] = read(sensor1);
    [accel2, gyro2, ~] = read(sensor2); % Read linear acceleration and angular
       velocity from MPU6050
    calibrationData1 = [calibrationData1; sensorReadings1]; %#ok<AGROW>
    calibrationAccel2 = [calibrationAccel2; accel2]; %#ok<AGROW>
    calibrationGyro2 = [calibrationGyro2; gyro2]; %#ok<AGROW>
end

% Compute offsets for sensors
offset1 = mean(calibrationData1, 1); % Offset for ADXL345
offsetAccel2 = mean(calibrationAccel2, 1); % Offset for linear acceleration (MPU6050
   )
offsetGyro2 = mean(calibrationGyro2, 1); % Offset for angular velocity (MPU6050)

% Adjust offsets to account for gravity on z-axis
offset1(2) = offset(1) - 9.81; % Subtract gravity from y-axis adxl
offsetAccel2(3) = offsetAccel2(3) - 9.81; % Subtract gravity from z-axis offset mpu
disp('Calibration complete.');

%% Data Collection
adxlData1 = [];               % To store ADXL345 sensor1 readings
mpuAccelData = [];            % To store MPU6050 linear acceleration readings
mpuGyroData = [];             % To store MPU6050 angular velocity readings
timestamps1 = [];             % To store timestamps for sensor1
timestamps2 = [];             % To store timestamps for sensor2
currentIndex = 1;             % Index for timeVec2 and pulseSignal2
```

```
% Start experiment
disp('Starting experiment...');
startTime = tic;             % Start timer

while currentIndex <= length(timeVec2)
    elapsedTime = toc(startTime); % Record the elapsed time

    % Check if it's time to apply the next pulse
    if elapsedTime >= timeVec2(currentIndex)
        % Apply the pulse signal to pin 6
        writeDigitalPin(arduinoObj, pulsePin, pulseSignal2(currentIndex)); % Set pin
            HIGH or LOW
    end

    % Read data from both sensors
    [sensorReadings1, tijd1] = read(sensor1);
    [accel2, gyro2, tijd2] = read(sensor2); % Read acceleration and angular velocity
        from MPU6050

    % Apply offset correction to all readings
    correctedReadings1 = sensorReadings1 - offset1;
    correctedAccel2 = accel2 - offsetAccel2;
    correctedGyro2 = gyro2 - offsetGyro2;

    % Store corrected data
    adxlData1 = [adxlData1; correctedReadings1]; %#ok<AGROW>
    mpuAccelData = [mpuAccelData; correctedAccel2]; %#ok<AGROW>
    mpuGyroData = [mpuGyroData; correctedGyro2]; %#ok<AGROW>
    timestamps1 = [timestamps1; tijd1]; %#ok<AGROW>
    timestamps2 = [timestamps2; tijd2]; %#ok<AGROW>

    % Move to the next pulse
    if elapsedTime >= timeVec2(currentIndex)
        currentIndex = currentIndex + 1;
    end
end

% Turn off the pulse pin after the experiment
writeDigitalPin(arduinoObj, pulsePin, 0);

disp('Experiment complete.');

%% Save Data
saveFileName = 'experiment_data_move_p1.mat';
save(saveFileName, 'adxlData1', 'mpuAccelData', 'mpuGyroData', 'timestamps1', '
   timestamps2', 'timeVec2', 'pulseSignal2');
disp(['Data saved to ', saveFileName]);
```

APPENDIX IX
IMPULSE RESPONSE STIFFNESS ESTIMATION

The stiffness impedance parameter has been estimated following a similar approach as Yagi et al. in [28, 29]. First we assume that the impedance of the joint can be modeled as a second order system described by:

$$\tau(t) = I\ddot{\theta}(t) + b\dot{\theta}(t) + k\theta(t) \tag{8}$$

Where $\tau(t)$ is the applied torque perturbation [Nm], I, b and k are the joint inertia [kgm2], rotational damping [Nms/rad] and rotational stiffness [Nm/rad] respectively. Furthermore, $\ddot{\theta}, \dot{\theta}$ and θ are the joint angular acceleration, velocity and position. Because a digital signal processor is used, a parametric linear difference equation is needed described as:

$$\theta_k = a_1\theta_{k-1} + a_2\theta_{k-2} + b_0\tau_k + b_1\tau_{k-1} + b_2\tau_{k-2} \tag{9}$$

Where a_1, a_2, b_0, b_1 and b_2 are the parameters that need to be estimated, and k is the time step. This equation can be rewritten ,with q being the shift operator, to get the mechanical impedance as:

$$\tau_k = \frac{1 - a_1q^{-1} - a_2q^{-2}}{b_0 + b_1q^{-1} + b_2q^{-2}}\theta_k \tag{10}$$

According to [30] the impedance in equation 9 can be related to equation 8 to get the impedance parameters such as the stiffness:

$$K = \frac{1 - a_1 - a_2}{b_0 + b_1 + b_2} \tag{11}$$

When the human joint is subjected to a force pulse input defined by:

$$\gamma_k = \begin{cases} \alpha, & (k = 0) \\ 0, & (k \neq 0) \end{cases}, \tag{12}$$

The resulting response is obtained as :

$$\theta_k = \alpha g_k \tag{13}$$

Here α is the magnitude of the force pulse input. With this the parameters a_1, a_2, b_0, b_1 and b_2 can be estimated with the following equation:

$$\phi = (G^TG)^{-1}G^T\Theta \tag{14}$$

Where

$$\begin{aligned} \phi &= [a_1 \quad a_2 \quad b_0 \quad b_1 \quad b_2]^{\mathrm{T}}, \\ \Theta &= [\theta_1 \quad \theta_2 \quad \theta_3 \quad \cdots \quad \theta_N]^{\mathrm{T}}, \\ G &= \begin{bmatrix} 0 & 0 & \alpha & 0 & 0 \\ \theta_1 & 0 & 0 & \alpha & 0 \\ \theta_2 & \theta_1 & 0 & 0 & \alpha \\ \theta_3 & \theta_2 & 0 & 0 & 0 \\ \vdots & \vdots & \vdots & \vdots & \vdots \\ \theta_{N-1} & \theta_{N-2} & 0 & 0 & 0 \end{bmatrix}, \end{aligned}$$

The constant α is calculated as followed:

$$\alpha = \frac{1}{T}\int_0^T \tau(t)dt \tag{15}$$

Where T is the duration of the torque pulse.

APPENDIX X
RAW DATA OVERVIEW

In Fig. 21. Can all the data from each participant and each trial per task be seen stacked over each other to show their distribution. The relax and resist task have already been filtered with a high-pass filter with a cut-off frequency of 0.5 Hz and show the perturbation in result of the applied force.

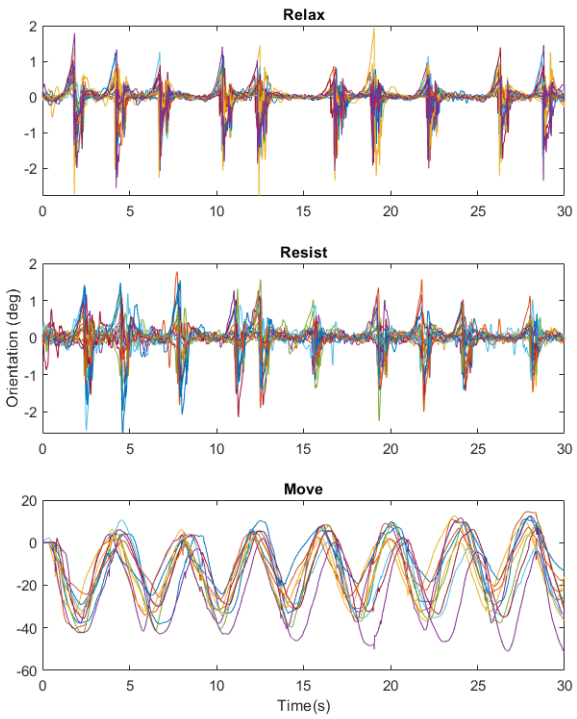

Fig. 21: Overview of the distribution of all the orientation data of the participants and trials per task. Each line represents a single trial that was recorded.

Fig. 22. Shows the distribution of the deflections of each participant and trial per task. Each perturbation signal had 10 perturbations, which resulted in 180 deflections recorded per task. The dashed vertical line represents the median and

Some of the recorded movement data of the move task was excluded due to human mistakes that were made. Either because the movement was out of synchronization with the metronome beat (a phase shift of $\lambda > 1.5s$), or because the movement was not a continuous sinusoidal movement but there was a wait time at the markings on the desk, as shown in Fig. 23. This resulted in a total of 4 trials that were excluded from the move task.

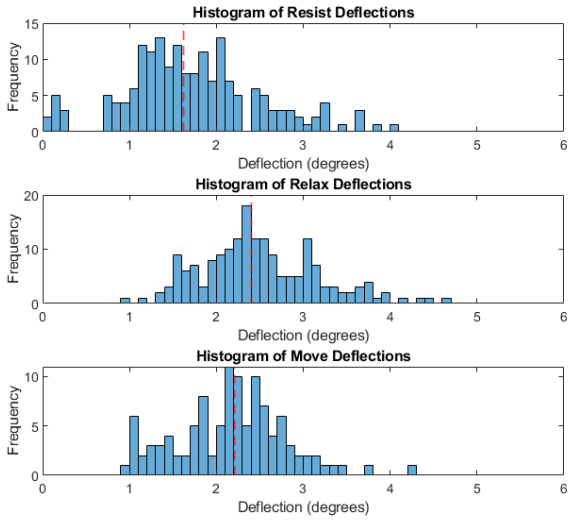

Fig. 22: Distribution of deflections per task. Dashed red line represents the median.

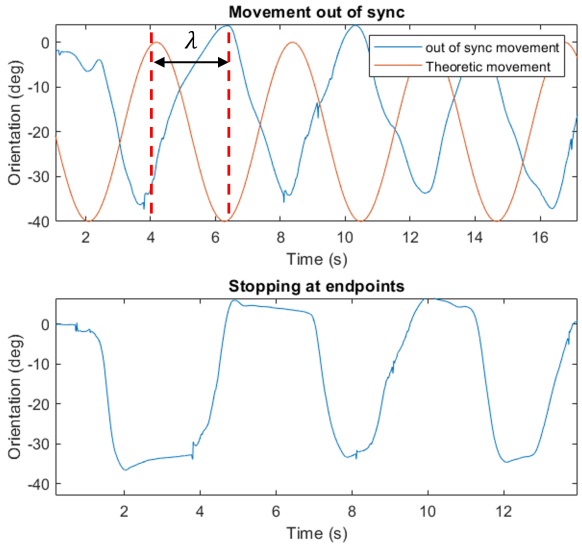

Fig. 23: In the top graph an example is show of a movement data set that was out of sync with the theoretical movement and therefore excluded. In the bottom graph an example of a movement that stopped at each end point and therefore excluded.

APPENDIX XI
TECHNICAL DRAWING SOLENOID BOX

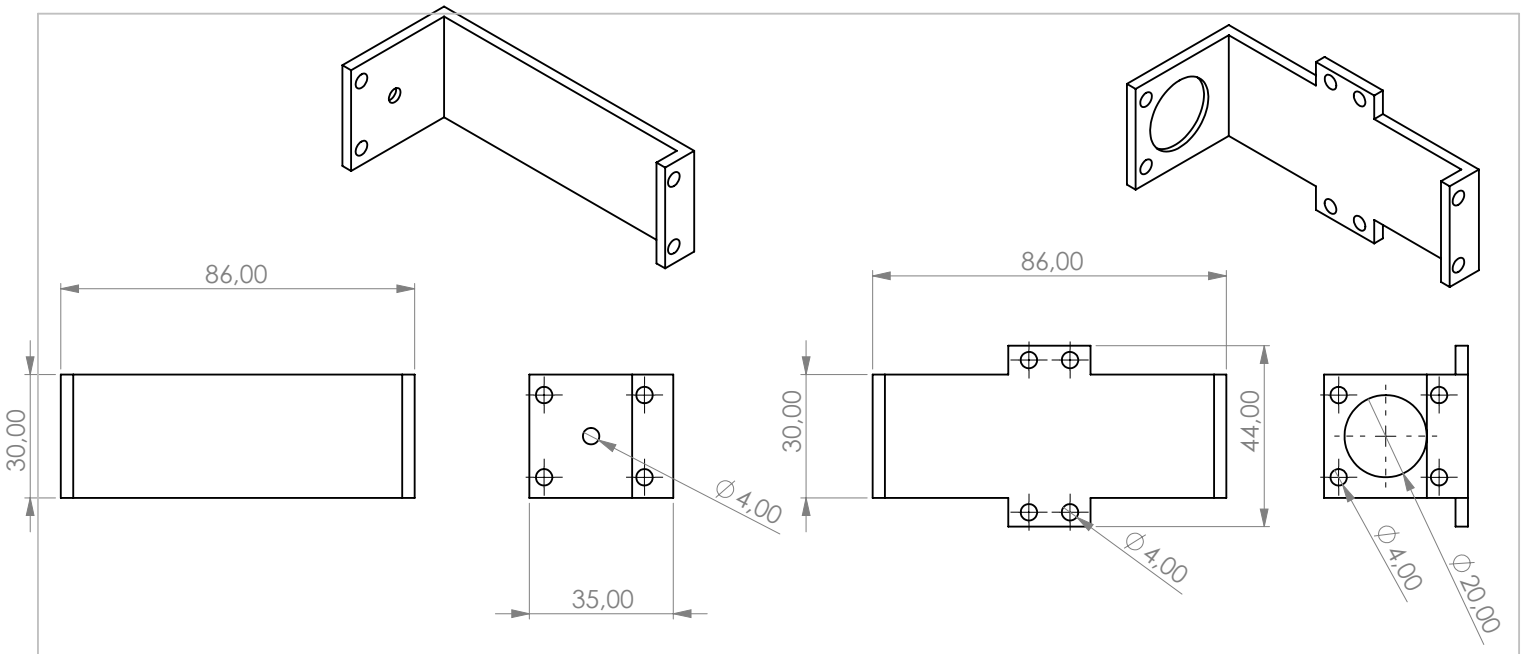

C:\Users\niels\OneDrive\Documenten\Graduation project\SW\proto\

TU Delft Delft University of Technology	name		units mm	scale 1:1.3	quantity 1	date 2-3-2025	remark
	Solenoid box		material pma				
		author Niels Doup			format A4	

APPENDIX XII
MATLAB CODE STIFFNESS ESTIMATION

```
clear
clc
close all
%%
load("orientation_results_relax_p2_trial2.mat")


%% Define the sample rate and filter parameters
sample_rate = 200;
cutoff_freq_low = 0.5;  % lower cutoff frequency (Hz)
cutoff_freq_high = 40;  % upper cutoff frequency (Hz)
hp_filter = designfilt('bandpassiir', ...
                       'FilterOrder', 4, ...
                       'HalfPowerFrequency1', cutoff_freq_low, ...
                       'HalfPowerFrequency2', cutoff_freq_high, ...
                       'SampleRate', sample_rate, ...
                       'DesignMethod', 'butter');


psi = filtfilt(hp_filter, (euler_angles(:,3)));
gamma = filtfilt(hp_filter, (euler_angles(:,1)));
a = asin((0.29*sin(deg2rad(gamma)) -0.0215*sin(deg2rad(psi)))/0.29);
a = rad2deg(a);
x = 0.29*sin(deg2rad(gamma));

%%
% Number of intervals
numIntervals = size(peakIntervals, 1);
k_values = zeros(numIntervals, 1);  % Preallocate k-values
alpha = -0.78;  % Constant based on torque pulse

% Loop over each interval
for j = 1:numIntervals
    % Extract the start and end indices for this interval
    start_idx = peakIntervals(j, 1);
    end_idx   = peakIntervals(j, 2);


    % Ensure the interval is within the bounds of euler_angles
    if end_idx > length(euler_angles(:,1))
        end_idx = length(euler_angles(:,1));
    end


    Theta = a(start_idx: end_idx,1);

    n = length(Theta);

    % Initialize the G matrix (n x 5)
    G = zeros(n, 5);

    % Fill in the first two columns:
    % For rows 2 to n, first column is Theta(i-1)
    if n >= 2
```

```
        G(2:end, 1) = Theta(1:end-1);
    end
    % For rows 3 to n, second column is Theta(i-2)
    if n >= 3
        G(3:end, 2) = Theta(1:end-2);
    end

    % Fill in the alpha entries along the diagonal of columns 3, 4, and 5
    G(1, 3) = alpha;
    if n >= 2
        G(2, 4) = alpha;
    end
    if n >= 3
        G(3, 5) = alpha;
    end

    % Compute phi using the least-squares solution
    % For numerical stability, we use the backslash operator:
    phi = (G' * G) \ (G' * Theta);

    % Compute k for this interval
    k_values(j) = ((1/(phi(3) + phi(4) + phi(5)))*(1 - phi(1) - phi(2)))*(180/pi);

end

% Display the estimated k values for each interval
disp('Estimated k values for each interval:');
disp(k_values);
mean_k = mean(k_values);
disp('mean');
disp(mean_k);
```